HHS Public Access

Author manuscript

Chem Eng Res Des. Author manuscript; available in PMC 2016 February 01.

Published in final edited form as:

Chem Eng Res Des. 2015 February 1; 94: 524–537. doi:10.1016/j.cherd.2014.09.014.

Plasma deposition of silver nanoparticles on ultrafiltration membranes: antibacterial and anti-biofouling properties

Mercedes Cecilia Cruz[a,1], **Gustavo Ruano**[b], **Marcus Wolf**[c], **Dominic Hecker**[c,d], **Elza Castro Vidaurre**[a], **Ralph Schmittgens**[c], and **Verónica Beatriz Rajal**[a,e]

[a]Instituto de Investigaciones para la Industria Química, Consejo Nacional de Investigaciones en Ciencia y Técnica y Facultad de Ingeniería, Universidad Nacional de Salta. Av. Bolivia 5150, A4408FVY Salta Capital, Argentina

[b]Centro Atómico Bariloche, CNEA, Av. Bustillo 9500, 8400, S. C. de Bariloche, Río Negro, Argentina

[c]Technische Universität Dresden – Institut für Festkörperelektronik, 01062 Dresden, Germany

[d]Fraunhofer-Institut für Elektronenstrahl- und Plasmatechnik, 01277 Dresden, Germany

[e]Fogarty International Center, University of California at Davis, U.S

Abstract

A novel and versatile plasma reactor was used to modify Polyethersulphone commercial membranes. The equipment was applied to: i) functionalize the membranes with low-temperature plasmas, ii) deposit a film of poly(methyl methacrylate) (PMMA) by Plasma Enhanced Chemical Vapor Deposition (PECVD) and, iii) deposit silver nanoparticles (SNP) by Gas Flow Sputtering. Each modification process was performed in the same reactor consecutively, without exposure of the membranes to atmospheric air. Scanning electron microscopy and transmission electron microscopy were used to characterize the particles and modified membranes. SNP are evenly distributed on the membrane surface. Particle fixation and transport inside membranes were assessed before- and after-washing assays by X-ray photoelectron spectroscopy depth profiling analysis. PMMA addition improved SNP fixation. Plasma-treated membranes showed higher hydrophilicity. Anti-biofouling activity was successfully achieved against Gram-positive (*Enterococcus faecalis*) and -negative (*Salmonella* Typhimurium) bacteria. Therefore, disinfection by ultrafiltration showed substantial resistance to biofouling. The post-synthesis functionalization process developed provides a more efficient fabrication route for anti-biofouling and anti-bacterial membranes used in the water treatment field. To the best of our knowledge, this is the first report of a gas phase condensation process combined with a PECVD procedure in order to deposit SNP on commercial membranes to inhibit biofouling formation.

[*]*Corresponding Author:* Verónica Rajal. INIQUI-CONICET. Buenos Aires 177. (A4402FDC) Salta Capital, Argentina. Phone: (+54 387)-4255347. Fax: (+54 387)-4251006. vbrajal@gmail.com.

[1]Present address: Singapore Centre on Environmental Life Sciences Engineering, Nanyang Technological University, Singapore 637551, Singapore

Keywords

ultrafiltration; biofouling; silver nanoparticles; plasma; gas flow sputtering; XPS

1. Introduction

The use of membrane technology has emerged as an invaluable tool in water purification process [1]. A disadvantage of this process is the biofilm deposition on the polymeric membrane surface that decreases the fluid flux and reduces its efficacy [2]. This deposition, known as biofouling, is one of the main problems limiting the widespread use of membranes in water treatment. Biofouling promotes increase in manufacturing and energy costs, damage or destruction of membranes, reduction in operating lifetimes, and secondary contamination of water by the metabolic products of microorganisms [2]. Different strategies have been proposed to address biofouling for example, feed-water pre-treatment, managing operational performance (flux, pressure, rinsing, chemical cleaning) [3], and development of modified antifouling membranes [2].

Among the membrane modification techniques developed to prevent fouling are, graft polymerization, plasma treatment, physical pre-adsorption of hydrophilic components, surfactant modification, ion electron beam, UV irradiation, and the incorporation of bioactive compounds or metal nanoparticles to act as bactericides [4–8]. In the last decade the use of nanomaterials has increased in membrane water purification [9–12]. In particular, silver has been considered as a potential disinfectant due to its intense antimicrobial activity and low toxicity to mammalian cells and tissues [13].

The exact antimicrobial action of silver nanoparticles (SNP) is not completely understood. Morones et al. [13] and Sondi & Sondi [14] suggested that SNP -in the range of 1 to10 nm- have three different antibacterial mechanisms of action: (i) attachment to the cell membrane surfaces drastically disturbing the permeability and respiration, (ii) penetration inside the bacteria and interaction with sulphur-and phosphorus-containing compounds such as DNA, causing further damage and (iii) release of silver ions, which also have a known bactericidal effect as reported by Feng et al. [15]. It is important to note that the release of silver ions is also involved in mechanisms (i) and (ii) and it is the definitive molecular toxicant under aerobic conditions [16].

Several researchers have incorporated SNPs on membranes by two distinct processes: (i) inside the casting solution of matrix during the membrane synthesis [17–23] and (ii) on the surface using different deposition processes [24–28]. Biofilm formation and the accretion of contaminants are expected to occur on the top skin layer of the membrane. Thus, modification treatments done on the surface are more promising than those made in the matrix. Further, they are cost effective since the use of reactive substances is reduced. Among the existing depositional processes, plasma is one of the most flexible technologies. However, the methods developed so far, require two stages for the generation and deposition of nanoparticles carried on in different devices, making the modification time consuming and increasing the probability of developing unwanted chemical reactions due to air exposure.

In this work a novel vacuum-based system is used for coating that allowed all modifications to be performed in a stepwise manner inside the same equipment; thus, preventing the exposure of the membranes to the atmosphere after each treatment. The aim of this study is to improve the efficiency of water disinfection process by developing membrane systems less susceptible to biofouling. Therefore, commercial polymeric membranes are activated with low-temperature plasma of different gases (Ar and Ar/O_2) and subjected to silver nanoparticle deposition by a gas flow sputtering (GFS) process. To enhance the fixation of the SNP we implement an intermediate process consisting in the deposition of a thin polymer film of poly(methyl)methacrylate (PMMA) by plasma-enhanced chemical vapor deposition (PECVD). The plasma-modified membranes are successful at improving the water disinfection process given their lower susceptibility to biofouling development. To the best of our knowledge, this is the first report of a gas phase condensation process combined with a PECVD procedure in order to deposit SNP on commercial membranes to inhibit the biofouling formation.

2. Materials and methods

2.1. Materials

Ultrapure water used in the experiments and in the preparation of solutions and suspensions was obtained by a commercial Milli Q system.

Ethanol, isopropyl alcohol, and hexane were provided by Sintorgan (Argentina). All chemicals were of analytical grade and used without further purification. The working gases argon and oxygen (Air Liquide, Paris, France) had 5.0 as purification grade. Methyl methacrylate (MMA) was purchased from Aldrich, with HPLC purification grade. For the experiments, the gas flow sputter source was equipped with two planar silver targets (250 × 80×10 mm). Silver plates had a purity of 3N5 and were purchased from Wieland Dental +Technik GmbH &Co.KG. Salmonella-Shigella Agar (SS, Britania) and mEnterococcus (BD, Difco) were used for cultivation of bacteria. Luria-Bertani (LB) Broth (1.0% tryptone, 0.5% yeast extract, 1.0% sodium chloride, pH 7.0) and Nutrient Broth (Britania) were used for *Salmonella* and *Enterococcus* culture, respectively. Membrane filtration and standard plate count methods were applied for determining live/viable bacterial numbers.

The membrane used was a commercial, flat-sheet type Polyethersulphone (PES) ultrafiltration membrane (OT050, OMEGA, Pall Corp., USA). According to the manufacturer, the Molecular Weight Cutoff (MWCO) was 50 kDa. This membrane was well characterized and had good performance for water disinfection with high efficiency for the removal of viruses, bacteria, and natural organic substances such as humic acids.

2.2. Membrane modifications

2.2.1. Plasma modification system—LB Nano (Figure 1) is a plasma process based on a novel approach for producing nanocomposites consisting of inorganic nanoparticles (NP) in either organic or inorganic matrix material. It was developed by the Technische Universität Dresden together with the Fraunhofer-Institut für Elektronenstrahl- und Plasmatechnik [29, 30]. Shortly, it consists of a NP source based on a gas phase

condensation (GPC) process and a reactive plasma process for the deposition of the matrix material. The separate generation of NPs and matrix material deposition allow for a versatile combination of both components. NP generation is based on an efficient hollow cathode sputter process and can be scaled up for large area coating.

The plasma reactor consists of the FAP VEA 200 electrode inside an aluminum housing that is differentially pumped against the recipient. The pressure in the plasma reactor is controlled by a capacitance manometer (MKS Baratron) and by a pendulum valve. The precursor is evaporated from a heated reservoir (vapor flow rates up to 50 sccm) and transported by argon (Ar) flux (vapor flow rates up to 100 sccm controlled by thermal mass flow controllers) into the reactor. It is a custom-made gas flow source based on the principle of a hollow cathode where the flow of inert gas carries atoms sputtered from the surface of two negatively charged targets facing each other out of the discharge zone. The sputtered atoms thermalize in the inert gas atmosphere and condense to form clusters and nanoparticles. In this case, working gases (Ar) are supplied via a mass flow controller to vary the gas flow from 1 to 5 slpm. By changing source parameters (e.g. pressure, power density of the targets) and drive speed of the rotary drive, nanocomposites of practically any useful thickness and particle concentration in the matrix can be obtained [30].

2.2.2. Membrane preparation prior to modification—Since commercial membranes have glycerin added at the end of the synthesis process to avoid drying, their pores could collapse due to the vacuum to which membranes are exposed to during the modification process. To remove glycerin from the porous membranes, consecutive washings with liquids from higher to lower surface tension were performed before modification treatment. Membranes were rinsed with bi-distilled water three times, and then immersed in water for three hours. After that, they were submerged consecutively in different organic solvent baths: ethanol, isopropyl alcohol, and hexane, with surface tensions of 22.27×10^{-3}, 21.7×10^{-3}, and 18.4×10^{-3} N/m, respectively. Once the solvent extraction was finished, membranes were stored in a dryer until use.

2.2.3. Membrane modification by plasma treatments—Silver nanoparticle deposition was carried out after two different processes of PES-membrane surface modification. The first was the activation of the surface with Argon (membranes M1, M2 and M3) and Argon/Oxygen mix (only membrane M4) plasma treatment (Table 1). The mix of Argon and Oxygen consisted on flows of 20 and 30 sccm, respectively. The second modification (on M2, M3, and M4) consisted of PMMA deposition by PECVD, after plasma activation. PMMA is an amorphous, transparent and resistant polymer with excellent optical clarity and was reported to show reduced nonspecific protein and peptide binding [31].

The thin film deposition of PMMA was done by the PECVD process with the following operation conditions: pressure 4 Pa, PMMA flow 5 sccm, Argon flow 40 sccm, power 100 W, pulse frequency 200 Hz, effective power 10 W, and deposition time 1 min.

The membranes (M1–M4) were subjected to SNP deposition, under the following conditions: power 3 kW, pressure in the aggregation zone 66 Pa, chamber pressure 10 Pa, and Argon flow 2 slpm. The deposition time was 20 s for M1 and M2 and 3 s for M3 and

M4. Under these conditions, SNP size and shape were measured by image analysis from Transmission Electron Microscopy (TEM, Tecnai T20, FEI). The LB Nano permits eight samples modifications during each run. Assays were repeated several times to obtain enough membranes for analysis.

It is important to note that each membrane modification was performed inside the same equipment, without removing the samples until the last deposition. Thus, there was no exposure to the atmosphere after plasma activation, thereby avoiding unwanted reactions.

2.3. Membrane characterization

2.3.1. XPS analysis and depth profiling—A VG XPS system using a standard ultra-high vacuum (UHV) chamber with a base pressure of 1×10^{-9} mbar was performed on the membrane samples to verify silver deposition. The spectra were recorded with a hemispherical electrostatic energy analyser (r = 10 cm) and Al Kα x-ray radiation (hν = 1486.6 eV). XPS analysis was also used to assess the fixation of SNP before and after washing assays and to determine if the addition of a PMMA layer was effective. The Ag subsurface distribution was also investigated by combining XPS with Ar bombardment to analyse the depth profiling. A beam of 1.5 keV Ar^+ ions was used, impinging in an angle of 60 degrees referred to the normal surface. The impacted area on the sample was approximately 1 cm^2. The total current on the sample (ions plus secondary electrons) was kept constant at 5×10^{-6} A. Slight charging of the surfaces was observed, shifting the peaks, without affecting the line shapes. The charge condition was monitored and later corrected by determination of the position of the Fermi edge before and after each measurement.

2.3.2. Scanning electron microscopy (SEM), contact angle and pore size—The surface morphology of the virgin–PES and prepared membranes were characterized by scanning electron microscope (JEOL JSM-6480LV). Membrane samples were first dried at 60 °C for 24 h and then coated with gold using a vacuum electric sputter coater (DESK - IV) before the SEM scan. The contact angle measurements were performed by the sessile drop method at room temperature, using a Standard Goniometer with DROPImage, Model 200-00 (Ramé-Hart Instrument CO). A drop (1 μl) of milli-Q water was placed onto the polymer surface using a micro syringe. The drop image was recorded by a video camera and digitalized. Ten measurements were made at different parts of each membrane. Average contact angle value, standard deviation, superficial energy and work of adhesion were calculated using the software provided by the manufacturer.

The mean pore size and the pore size distribution of membrane samples were measured using gas-liquid displacement porometry (GLDP) with the Porolux 1000™ capillary flow porometer (POROMETER nv). Porefil (Benelux Scientific) wetting fluid with a surface tension of 16 $dyn.cm^{-1}$ was used to wet the membrane prior to the measurements. The final pressure measurement was set to 10.5 bar. The mean pore diameter was calculated from the mean flow pressure, which corresponds to the intersection of the wet curve with the calculated half-dry curve (dry and a wet run). The pore size distribution was later calculated by the processing software (Benelux Scientific, Belgium).

2.3.3. Ultrafiltration system and membrane permeability—Ultrafiltration experiments were carried out in a lab-scale flat-sheet tangential-flow system at room temperature. The main advantages of this type of system (in all scales) are, the tangential flow decreases the polarization concentration and the fouling of the membrane, the cells are easy to clean, and the replacement of used membranes is relatively easy. A custom-designed cell module was used. It consisted of a 1 l feed tank containing the water matrix solution (milli-Q water or PBS 1×), with or without microorganisms depending on the experimental requirements, and an UF stainless steel circular cell. The effective membrane area was 9.0×10^{-3} m^2. A peristaltic pump (APEMA, BS6D) with variable feed flow kept the pressure constant. The feed solution was maintained at room temperature and fed directly to the membrane side of the cell through the pump. The retentate was recirculated, while the permeate fluid was continuously discharged. The permeate fluid was weighed by an electronic balance (Shimadzu UX-2200H, Japan), which was serially linked to a computer for automated data collection at 1 min intervals.

Compaction of each membrane was done for 1 hour at 2 bar of pressure. Then, the hydraulic permeability (L_h) with milli-Q water was obtained at 0.5, 1.0, and 1.5 bar. L_h ($l.m^{-2}\ h^{-1}.\ bar^{-1}$) was determined using the equation $L_h = J/\Delta p$, where J is the flux ($l.m^{-2}\ h^{-1}$) calculated as $J = V/A\ \Delta t$. The pure water flux (J_0) of the membrane was in the stabilized state. The collected permeate volume (V, ml) was adjusted to 20 °C as reference temperature to account for the viscosity change of water in order to obtain the volumetric flux [32]. The characteristic pore structure factor ($PSF = \varepsilon_p/l_p$) was calculated from the membrane hydraulic permeability coefficient L_h, measured directly from pure water permeation experiments, according to the Hagen–Poiseuille pore flow model:

$$L_h = \frac{r^2 p}{\varepsilon_\mu} \frac{\varepsilon_p}{l_p} \quad (1)$$

where μ is the viscosity of pure water (assumed to be 0.001 Pa·s at room temperature), l_p is the average thickness of the deposited layer (measured from SEM images) and ε_p is the porosity. The increase in the pore structure factor reflects either the increase in skin layer porosity or the decrease in skin layer pore length, or a combination of both [20].

2.4. Evaluation of antibacterial and anti-biofouling properties

Several tests were carried out in order to characterize the antibacterial and anti-biofouling properties of the modified membranes.

2.4.1. Suspension preparation—Membrane anti-adhesion and anti-bacterial tests were conducted with pure cultures of *Salmonella enterica* var. Typhimurium (as a model for Gram-negative bacteria) and *Enterococcus faecalis* (as a model for Gram-positive bacteria). *Salmonella* were first cultured in a flask containing 10 ml of Luria Bertani (LB) broth at 37 °C in a shaking incubator (Dalvo) for 24 h. Meanwhile, *E. faecalis* were cultured at 41°C for 24 h in nutrient broth. Next, the biomass of each culture was separated from the broth by centrifugation at 4,000×g (Microcentrifuge, Eppendorf) for ten minutes at 4 °C and the supernatants were discarded. Phosphate buffered saline (PBS) was added to each pellet, which was vortex mixed to homogenize it. The suspension was centrifuged again to separate

bacteria from PBS. This procedure was repeated three times to ensure the removal of all remaining nutrients from the broth and to prevent further growth of bacteria during the anti-adhesion test [26]. The final suspensions of *Salmonella* and *Enterococcus* were diluted with PBS to reach concentrations of approximately 10^7 and 10^4 CFU/ml, respectively.

2.4.2. Adhesion tests and antibacterial characteristics—For adhesion tests, 100 mm^2 of each type of membrane was immersed into the *Salmonella* suspension (10 ml) in a 100 ml sealed bottle. The mixture was incubated on an orbital shaker at 200 rpm and 37 °C for 5 h. Next, the membranes were taken out and rinsed gently with PBS, three times to remove both loosely attached and planktonic bacteria from the surface. According to Liu et al. [26], fixation of adhered bacteria is needed prior to the SEM scan. Thus, membrane samples were first immersed into 2.5% (v/v) glutaraldehyde-buffer phosphate solution at 4 °C for 5 h. Later the membranes were subjected to dehydration steps with 25, 50, 75, and 100% ethanol and then dried at 30 °C to be ready for the SEM scan. The bacteria remaining on the surface of each membrane (attached bacteria) were then observed with SEM as an indication of bacteria adhesion. All pictures were taken with 3,000× magnification and 20 kV voltage. The same procedure was carried out with the *E. faecalis* suspension.

Standard plate count and membrane filtration methods were used to estimate the number of viable *Salmonella* and *Enterococcus* remaining in the suspensions (after the membranes with the adhered microorganisms were removed). To accomplish this, in the case of *Salmonella* 100 μl of 10-fold serial dilutions of the suspensions were cultured in SS agar at 37 °C for 24 h using the spreader technique. For *Enterococcus* 1 ml of 10-fold serial dilutions were filtered and the filter was transferred to mEnterococcus Agar in Petri dishes and incubated at 35 °C for 48 h.

Antibacterial properties in a static state (non-stirred contact) were also evaluated. A small volume (30 μl) of the *Salmonella* suspension was spiked onto both untreated (used as control) and silver-coated membranes (100 mm^2 chips), which were incubated at room temperature for 0, 0.25, 2, 6, 12, 18, and 24 h. After each incubation time, two controls and two silver-coated chips were removed from the bacterial suspension, added to a tube containing 5 ml of 1× PBS and vortex mixed for 30 s to detach bacteria from the surfaces. The number of viable bacteria was evaluated by colony counts in SS agar plates and expressed as log(CFU/chip) [33].

2.4.3. Disinfection and anti-biofouling characteristics—Membrane performance was also evaluated during disinfection by ultrafiltration of 1 L of PBS spiked with *Salmonella* (10^6 CFU/ml) and *Enterococcus* (10^5 CFU/ml). In all these experiments the transmembrane pressure was set to 1 bar. Fluxes were normalized (divided by J_0) to compensate for the existing differences in the initial values and to compare between different assays. The efficiency of bacteria removal was measured in terms of the log removal value (LRV), which is the logarithm to base 10 of the ratio of bacteria concentration in the feed solution to that in the permeate. The flux reduction (RF) as a typical fouling characteristic was described by the following equation:

$$RF = \left(1 - \frac{l_p}{l_0}\right) \times 100\% \quad (2)$$

3. Results and Discussion

3.1. Surface composition by X-ray photoelectron spectroscopy (XPS) analysis

XPS allowed the identification of the elements that constitute the membrane surface. The present work was devoted to characterizing the amount of Ag at the membrane surface. Detailed spectra acquired shared the same features for Ag 3d and C 1s peaks, as shown in Figure 2 for M4. The range of binding energies for C 1s showed clearly the existence of two independent components. A fitting of the spectrum with appropriate Doniach-Sunjic functions [34] after Shirley-type background subtraction allowed the separation of the spectra into the contributions of the photoelectrons coming from two types of carbon atoms in the samples. One was attributed to C atoms bound to either other C or H atoms (double hatched component centered at 285.1 eV) and the other to C atoms bound to oxygen atoms (simple hatched component centered at 288 eV) [35].

On the other hand, the spectrum for Ag 3d (Figure 2) depicted a couple of peaks separated by about 6 eV, corresponding to the spin-orbit splitting of the level 3d into 3d 5/2 and 3d 3/2. Additionally, the ratio of intensities between the Ag 3d 5/2 and Ag3d 3/2 was 2/3 as expected for a d spin-orbit splitting. The fitting of this spectrum, using the above-mentioned parameters, indicated just one component centered at 368.4 eV, which corresponds to metallic Ag [36]. The Ag 3d to C1 s ratio can be taken as a measure of the amount of Ag deposited on each membrane. However, to eliminate the adventitious C -generally present on the surfaces- which contributed to the spectrum at around 285 eV, the ratio between the areas of Ag 3d (A_{Ag}) peak and the C-1s (A_C) subcomponent at 288 eV was used.

In order to characterize the dispersion of Ag nanoparticles in the near surface region of the membranes a depth profiling was performed for each of them (Figure 3). Curves are shown normalized to the maximum values, and the sputtering time was proportional to the thickness removed by the bombardment. It is apparent that in the M2 sample the Ag was spread to a slightly larger extent in depth with respect to samples M3 and M4. However, the major difference in the Ag deposition profiles was between sample M1 and the rest of the set. In membrane M1, without deposition of PMMA, the Ag was concentrated in a shallow region.

In addition, the shape of the silver nanoparticles was confirmed as spherical under the deposition conditions used, after which the particle size was measured by TEM imaging (Figure 4). A bimodal - particle size distribution, fitted by two Gaussian curves, was obtained, with average diameters of 2.7 ± 0.7 and 3.6 ± 1.3 nm, estimated by measuring the perimeter of 100 randomly selected particles. It is important to note that a silver nanoparticle size less than 5 nm diameter appears to be a major determinant of particle toxicity. Due to the larger specific surface area available for interaction, the smaller particles exhibit greater antimicrobial activity than larger particles [37]. Hence, the small SNP size obtained in this work show a high bactericidal behavior, as discuss in section 3.4. Furthermore, the redox

potential of releasing silver ions depends on the size of the nanoparticle. The redox potential is more positive as the size increases. According to $Ag_n \leftrightarrow Ag^+ + e^-$, when $n = 1$ (free silver atom) the potential is −1.8 V and when $n \rightarrow \infty$ the potential is 0.799 V [38].

3.2. Membrane surface modifications

The Ar/O_2 plasma treatment had a dramatic influence on the surface morphology of the treated membranes. The hydrophilicity and permeability increased remarkably, while the rejection decreased due to the opening up of more pores or the elimination of the skin layer (Figure 5). These results are in agreement with the existing literature [8, 33]. When etching occurs the membrane becomes thinner and the flux increases consequently [7]. The etching effect was detected in the SEM image of a membrane, treated with Ar/O_2 plasma without polymer deposition (Figure 5). It revealed a more porous surface with severe damage of the uppermost portion of superficial layer. It is known that O_2 plasma etches the organic material through ashing reactions due to the oxidation of surface functional groups to volatile gases [25]. To control this damage, we proposed the addition of a thin PMMA polymer deposition to improve the performance of the membrane.

Plasma surface treatment was chosen due to its advantages: i) it is a very fast and economic process performed at room temperature and ii) it modifies the polymer surface structure selectively while the bulk properties remain largely unaffected [39]. Currently, UF membranes made of synthetic polymers are more commonly used in water treatment. PES is one of the most frequently used compounds in membrane synthesis, despite being a hydrophobic polymer. This can be attributed to its high resistance to cleaning reagents (such as hypochlorite and sodium hydroxide) and the fact that it can be used over a wide pH range [40].

The plasma procedure led to altered surface chemistry of the PES films. These alterations depend on the gas used for the surface modifications, as also noted in literature [8, 40–42]. Thus, it is plausible that during the membrane activation with plasmas, containing simple non-carbon gases (such as Ar or O_2), the molecular bonds of the superficial layer, such as C—C and C—H, are cleaved resulting in desaturation of the carbon chain. Due to the type of plasma equipment used, without exposure to the atmosphere, it was not possible to analyze those chemical groups created after each individual stage.

A PES membrane surface contains sulphone, aromatic and ether groups [40]. According to Gröning et al. [41] argon plasma on PES membranes has the following effects: i) induces the reduction of the sulphonic group ($-SO_2-$) to sulphide, ii) attacks mostly the oxygen in the sulphonic group, and iii) produces a loss of oxygen from the ether group. It can also produce a graphitization of the polymer surface due to dehydrogenation of the phenyl ring. However, this process is only observed after prolonged periods of treatment. With Ar/O_2 plasma a large number of chemical reactions are possible resulting in a very oxidized PES surface [40, 42]. Argon/oxygen plasma treatment leads to the formation of hydroxyl, carbonyl, and carboxyl groups on the polymer surface and etching. Thus, PMMA was added to: i) cover the enlarged pores caused by etching due to plasma treatment, ii) keep the hydrophilicity reached by plasma activation [8], and iii) increase the fixation of SNPs. Furthermore, we

proposed that activation with Ar or Ar/O_2 plasma enhances the adhesion of PES and PMMA.

3.3. Membrane characterization

3.3.1. Assessment of the fixation of SNP by PMMA thin layer addition—Fixation of SNP onto membrane surfaces after addition of a thin layer of PMMA was assessed by permeating 1 L of milli-Q water through the membranes in a tangential flow cell (4 to 5 hours depending on the permeability of each membrane). The amount of SNP before and after the washing was calculated as the ratio of the area under the doublet Ag 3d to that of C 1s (A_{Ag}/A_C) determined by XPS. A significant percentage of SNP was washed out from the membrane.

The initial (before washing) A_{Ag}/A_C ratios over the surface were 15.94 and 13.44 for M1 and M2, respectively, which correlate to the conditions used during the deposition in their preparations (power 4 kW, pressure in aggregation zone 45 Pa and SNP deposition time 20 s). However after washing, the loss of Ag for sample M1 (9.76) was more than the double than for M2 (4.29), suggesting that the aggregation of a thin layer of PMMA increased the fixation of the SNP on the membrane surface. The amount of Ag for M3 and M4 prior to washing was similar (4.82 and 4.67, respectively). This was expected since they were subjected to the same deposition conditions (SNP deposition time 3 s). Also, the amount of Ag lost, upon washing, for M3 and M4 were almost similar to M2.

In addition, to assess the effect of washing on each sample, a depth profiling of the Ag 3d to C 1s ratio (A_{Ag}/A_C), normalized to its maximum value, was performed (Figure 6). The normalization was done to analyze the uniformity of the loss of Ag. In membranes treated with PMMA (M2 and M4) the washing produced a uniform decrement of Ag in the profile (Figure 6, B and C, respectively). Conversely, M1 (without PMMA, Figure 6, A) exhibited a very broad profile, with an increased quantity of Ag in the interior of the membrane and some depletion in the surface (inset). This change in the profile was indicative of a diffusion process occurring during the washing. In addition, it demonstrated the immobilization effect of the PMMA on SNP fixation (M2 and M4).

It is important to note that the slight increment of the permeability in M2 (47 ± 1.7 l.m^{-2}·h^{-1}.bar^{-1}) was probably due to pore blockage in M1 (30 ± 1.5 l.m^{-2}·h^{-1}.bar^{-1}), resulting from the diffusion of nanoparticles inside the membrane. In M2 diffusion of SNPs into the membrane was prevented by the deposition of the polymer (Figure 6, A, B).

This new fixation technique represents a novel method that allows us to concentrate the silver onto the membrane surface and maintain it there. This in turn maximizes the efficiency of the membrane during filtration. Since the incorporation of PMMA led to the successful fixation of SNP, only the results from membranes M3 and M4 were analyzed in the following sections. Those membranes (M3 and M4, prepared using a lower SNP deposition time (3 s), demonstrated higher permeability than M2 (20 s deposition time).

Finally, Ag concentration was assessed in the permeate water by optical ICP (Perkin Elmer). It was in all cases under the method detection limit (< 0.01 ppm), and below the standard

limit established by WHO [43] for silver concentration in drinking water (0.1 mg Ag/l). According to the World Health Organization, a concentration of silver in drinking water of up to 0.1 mg Ag/l (a concentration that gives a total dose over 70 years of half the human NOAEL of 10 g) poses no significant health risk.

3.3.2. SEM and XPS spectra—We analyzed the surface morphology of the virgin PES and of the treated membranes by SEM. Membranes M3 and M4 showed smoother surfaces compared to an untreated membrane (Figure 7), probably due to PMMA deposition by PECVD. Less surface roughness is a crucial factor in decreasing membrane fouling. It is expected that the performance of treated membranes is inversely proportional to the adhesion level and biofouling [28]. The roughness of modified membranes was reduced by SNP deposition because the particle size (lower than 4 nm) was smaller than the membrane pore size. It is important to note that according to EDS analysis, the spheres observed on membrane surfaces had the same composition as the surface, thus they were not silver nanoparticles. Furthermore, an external survey of the membranes showed another characteristic of silver deposition, the color change from the original white to yellowish in the prepared membranes, which persisted even after washing tests.

The XPS spectra (for M3 and M4 in Figure 7, right side) revealed the presence of Ag, C, and O. The Ag peaks were clearly observed in the samples with deposited SNP. Conversely, they were completely absent in the spectrum of the virgin membrane. Both O and C were constituents of the PES membranes and also of PMMA. However, small amounts of these compounds were unavoidable due to the contamination during the exposure to the atmosphere. N 1s signal, which varied in intensity in different samples, was always low, and may indicate the presence of air trapped in the porous structure of membranes.

3.3.3. Morphological and transport properties—The water contact angles for both treated membranes (M3 and M4) were lower than for the virgin membrane (Table 2). These measurements denote the hydrophilic character of PMMA related to the contributions of dipole–dipole and induced dipole–dipole interactions [44]. A wet high-energy surface allows the drop to spread, reducing the contact angle. These reductions lead to a higher hydrophilicity but not to a higher permeability. Membranes with SNP exhibited lower fluxes, probably related to the presence of the PMMA deposited layer and to SNP themselves as additional barriers. In general, the resistance to flow of a membrane increases together with the thickness causing decreased flux [27]. Also, the agglomeration of SNP could cause plugging of membrane pores, although the SNP size was very small compared to pore sizes.

Membrane pore size is considered one of the main factors in assessing the membrane separation performance. The pore size distribution is expected to be a determining factor as to which molecules or particles would be retained and which ones would pass through the membrane. However, the superficial characteristics of the membrane also play a crucial role and the expected behavior could change when reactive components (such as SNP) are on the membrane surface. The unmodified membranes had smaller pores than the modified ones (Table 2). The first step of plasma activation with different gases could have produced etching of the membranes leading to larger pores for PMMA and SNP depositions. Although

deposition time of PMMA and SNP were the same for both membranes, the different effect of plasma activation on PES could be responsible for the different pore size and length. Figure 8 showed a deeper penetration of PMMA inside the pores due to greater modification caused by Ar/O_2 plasma. The deposited layer in M3 was denser than in M4. The amount of PMMA deposited was the same for both membranes (same plasma conditions and time of exposure). However, in M4 the layer was thicker since the polymer was able to penetrate deeper into the pores.

This increment of the effective permeation region explains the higher permeability and selectivity for M4 over M3 (Figure 8, A, B). Also, it seems that the PMMA layer in M4 is less dense due to its high compaction factor, its slightly higher permeability compared to M3, and the PSF is almost three times the value for M3 (Table 2). Furthermore, in M3 the distribution of PMMA generated a dense layer with more tortuous pores leading to a lower permeability.

The results showed a larger pore size of prepared membranes, almost 2-fold for M3 compared to PES membrane. It was also observed that the porosity (number of pores and connections between them) was lower. Porosity (ε) was calculated from Eq. 1 ($\varepsilon_p = PSF \times l_p$), considering l_p as the thickness of the selective or active upper layer of polymerized PMMA (Figure 8). The ε values were 2.15×10^{-4} and 1.12×10^{-3} for M3 and M4, respectively. According to Hagen-Poiseuille model, based on the dependence of the flow on pore radius (4- to 16- times if the porosity was constant), the permeability for M3 was expected to increase. However, due to the decrease in porosity (and therefore of the PSF, Table 2) the permeability was lower for M3 than for M4. The deposition of PMMA and the presence of nanoparticles might affect the porosity, tortuosity, pore size of the membrane skin and the macrovoid morphology of the asymmetric support layer. This last property is important in view of the membranes' compaction behavior [45].

The pore size distribution was determined using porometer analysis based on the bubble point method (Figure 9). The samples with liquid-filled pores were subjected to a pressure increase by a gas source. The pores were uniformly distributed for both treated membranes. However, two peaks that do not differ significantly were observed for M4 (0.997 μm and 0.947 μm, the highest peak). The pore size distribution also showed that the percentage of smaller pores in M3 was very low. This implies that most of them were clogged by PMMA, which may significantly affect the calculated porosity.

3.4. Evaluation of antibacterial and anti-biofouling properties

3.4.1. Adhesion tests and antibacterial characteristics—The attachment of Gram-negative and Gram-positive bacteria to the membrane surface was assessed with suspensions of *S*. Typhimurium and *E. faecalis*, respectively. After 5 h of incubation of the membranes (100 mm^2) in the bacterial suspensions, the bacteria that remained on each type of membrane were observed by SEM for adhesion tests. No biofilm was observed on SNP-membranes for both types of microorganism (Figure 10, B, C, E, F), while *S*. Typhimurium significantly adhered to the virgin membrane (Figure 10, A). The lower adhesion of *E. faecalis* to the untreated membrane (Figure 10, D) could be related to the original surface modification made by the manufacturer of the commercial membrane.

Since Gram-positive bacteria cell walls have 3–20 times more peptidoglycan than Gram-negative, it was expected that the bactericidal property of SNP have a greater effect on *S.* Typhimurium. However, in this study the effect was similar for both bacteria, indicating that the SNP size (< 4 nm) deposited was effective in hindering the viability of the microorganisms assessed. According to Choi and Hu [37] silver nanoparticle size less than 5 nm could be more toxic to bacteria than any other fractions of nanoparticles. The lower adhesion found could be attributed not only to SNP, but also to the higher hydrophilicity of modified membranes (see Table 2, in terms of water contact) [26].

The bactericidal performance of treated membrane was also assessed. Suspensions of 1×10^6 *S.* Typhimurium cells per ml and 2×10^4 *E. faecalis* cells per ml were put in contact with SNP-membranes for 5 h at 200 rpm and then cultured to count viable bacteria. There was no bacterial growth from the suspensions that were in contact with SNP-membranes, in contrast to the results with the suspensions in contact with virgin membranes (Figure 11). This proves the bactericidal effect of the SNP on both Gram-positive and Gram-negative bacteria.

A contact test (static, non-stirred) was performed with *S.* Typhimurium, in order to assess the effectiveness of the deposited SNP and to avoid the action of silver released. The *Salmonella* counts on untreated membranes remained essentially the same throughout the 24-h exposure period (Figure 12). In contrast, the bacterial counts on SNP-deposited polymeric membranes began to decline after only 15 minutes. After a 2-h exposure of membrane M4, no colonies were counted, while the reduction for M3 at this time was over 2-logs. No viable bacteria were detected on either type of modified membranes after 6 hours of contact. Thus, silver nanoparticles deposited on the surface not only prevented biofouling but also inactivated bacteria.

It is known that biofilm formation starts with cell adhesion to the membrane surface and progresses with the accumulation of microorganisms, including thick layers of extracellular polymeric substances (EPS), other organic compounds, and finally the development of a complex community of microbial cells [17, 24, 46]. To avoid difficulties in eliminating the bacteria once they are established, it is better to prevent the initial adherence for controlling biofilm growth. The results of the different anti-adhesion tests carried out confirmed that a biofilm formation was prevented by the SNP-membranes.

When the membrane comes in contact with water and is colonized by bacteria a biofilm layer on a membrane surface is formed inevitably. Hence, membrane units in water treatment are excellent systems for biofilm development and biofouling is the most significant issue to address. These experiments demonstrated that membranes M3 and M4 exhibit potent bactericidal properties against Gram-positive and Gram-negative bacteria. Both membranes showed biofouling resistance since microorganisms were less likely to attach when the membranes were exposed to cell suspensions. Also, *S.* Typhimurium was completely inactivated within 6 hours of exposure when deposited onto the membrane surface. The strong antibacterial activity of treated membranes observed in these experiments was in agreement with other silver functionalization studies on different polymeric membranes of polyamide [27], cellulose acetate [26], polypropylene [28],

polyacrylonitrile [12], polyethersulphone [23] and polysulfone [17, 18], by various modification processes.

3.4.2. Disinfection and anti-biofouling characteristics measurements—

Membrane performance in terms of permeability and efficiency of bacterial removal was evaluated during disinfection by ultrafiltration of 1 l of PBS solution spiked with *S.* Typhimurium (1×10^6 CFU/ml) and *E. faecalis* (1×10^5 CFU/ml).

UF was performed with each membrane to compare the flux between the three membranes. The flux of the virgin membrane was higher than that of the modified ones; although it started to decline after 50 min of use and decreased more than 30% during the operation time (Figure 13). On the other hand, the flux remained almost constant until the end of the filtration for M3 (200 min) and for M4 (160 min), in both cases maintaining more than 80% of the initial value. It is possible that the higher permeability of the untreated membrane allowed convective transport of foulants across the membrane surface, inducing a more pronounced biofouling. Biofouling causes unacceptable operational problems, and generally occurs when the flux decrease exceeds 15% of the start- up values. When the installation reaches this situation corrective actions are recommended [46]. The results obtained with the treated membranes showed that the lifetime of membranes may be enhanced due to the anti-biofouling properties of Ag. The stable fluxes obtained indicate that lower frequency of backwash or cleaning procedures would be needed, making the process more economical and long-lasting. Even though the flux of the treated membranes was lower than for the virgin membrane, improvements such as the constant permeability and anti-biofouling ability were achieved.

The efficiency of bacterial removal was measured in terms of the log removal value (LRV). Rejection (-log removal) was 4.7 and >7.6 for M3 and M4, respectively, and 6.2 for the untreated membrane. The lower LRV of M3 could be attributed to the larger pore size (0.1387 μm), to its bubble point pore size (1.556 μm), and to the greater loss of silver compared to M4. There was full removal (100%) of *E. faecalis* for all membranes (treated and untreated) due to the shape and a larger diameter (1 μm) of Gram-positive microorganisms compared to *S.* Typhimurium width (0.5 μm).

SEM images were obtained to verify the attachment of bacteria to the membrane after UF assays (pictures not shown). M3 showed the less-fouled surface, due to its higher hydrophilicity (lowest contact angle, Table 2) and lower flux (Figure 13), that allowed for lower foulants transport. It is worth mentioning that although bacteria can be observed on the surfaces of both prepared membranes, the attached cells were not viable. After UF, a piece of each fouled membrane (1/4 disc) was placed on Petri dishes with SS and ME agar to observe the growth of viable *Salmonella* or *Enterococci* bacteria, respectively. After 24 h of incubation there was no colony development from M4 and only a non-significant small amount grew on M3, while virgin membranes were fully colonized. Even though it was found that the SNP reduction (or loss) during the ultrafiltration was high, it is clear that the remaining nanoparticles on the surface maintained the bactericidal activity and reduced biofilm formation. Furthermore, Taurozzi and co-workers [18] found that the significant loss

of silver was potentially advantageous for downstream inhibition of biofilm (test organisms *E. coli*).

4. Conclusions

In the present study, a technique was developed for plasma deposition of silver nanoparticles on commercial polymeric membranes and key improvements were achieved in membrane performance.

- Silver was deposited on the surface, where the biofouling formation process takes place. This resulted in a more efficient utilization of SNP, thus reducing production costs. Also, the equipment and procedure used are easily scalable. The depth profiling analysis by XPS allowed the study of evolution and transport of silver concentrations on the surface and in-depth of modified membranes. This provides an interesting assessment in the study of membranes with nanoparticles.
- Ar/O_2 (M4) plasma activation led to better SNP fixation, permeability, and antibacterial property than Ar plasma activation (M3). Also, the aggregation of a thin layer of PMMA was important for SNP fixation (M2, M3, M4).
- Silver nanoparticles played a crucial role by increasing substantially the resistance of treated membranes to biofouling. This resulted in a significant decrease in the colony counts in the surrounding suspension and on the membrane surface for both microorganisms (Gram-negative and Gram-positive).
- The Ar/O_2 plasma-activated membrane (M4) was successful at improving the water disinfection process and prolonging membrane lifetime, given its lower susceptibility to biofouling development. The new membranes seem promising to be applied in the field of water treatment.
- Further work is needed in order to improve the permeability and SNP fixation of these modified membranes and also to study the behavior under actual operational conditions (with real water samples) for longer periods of time.

Acknowledgments

This project was supported by the Scientific and Technological Cooperation Program between the Secretaría de Ciencia, Tecnología e Innovación Productiva (SECyT, Argentina) and the German Academic Exchange Service (DAAD, Germany) project code DA0704. It was also partially supported by NIH Grant D43 TW005718 funded by the Fogarty International Center and the National Institute of Environmental Health Sciences (USA). Mercedes Cecilia Cruz and Gustavo Ruano were supported by CONICET fellowships. The SEM micrographs were taken in the Laboratorio de Microscopía Electrónica de Barrido (LASEM) - ANPCyT UNSa CONICET- Salta.

References

1. Schrotter, J-C.; Bozkaya-Schrotter, B. Current and Emerging Membrane Processes for Water Treatment. In: Peinemann, K-V.; Nunes, SP., editors. Membranes for Water Treatment. WILEY-VCH Verlag GmbH & Co. KgaA; Weinheim: 2010.
2. Chen, V.; Mansouri, J.; Charlton, T. Biofouling in Membrane Systems. In: Peinemann, K-V.; Nunes, SP., editors. Membranes for Water Treatment. WILEY-VCH Verlag GmbH & Co; Weinheim: 2010.

3. Gao W, Liang H, Ma J, Han M, Chen Z-l, Han Z-s, Li G-b. Membrane fouling control in ultrafiltration technology for drinking water production: A review. Desalination. 2011; 272:1–8.
4. King S, Escobar I, Xu X. Ion beam irradiation modifications of a commercial polyether sulfone water treatment membrane. Environmental Chemistry. 2004; 1:1–5.
5. Van der Bruggen B. Chemical Modification of Polyethersulphone nanofiltation Membranes: A review. Journal of Applied Polymer Science. 2009; 114:630–642.
6. Goddard JM, Hotchkiss JH. Polymer surface modification for the attachment of bioactive compounds. Progress in polymer science. 2007; 32:698–725.
7. Cho DL, Kim S-H, Huh Y, Kim D. Efects of surface modification of the membrane in the Ultrafiltration of waste water. Macromol. Res. 2004; 12:553–558.
8. Wavhal DS, Fisher Er. Hydrophilic modification of polyethersulphone membranes by low temparature plasma-induced graft polymerization. Journal of Membrane Science. 2002; 209:255–269.
9. Savage N, Diallo MS. Nanomaterials and water purification: Opportunities ans challenges. Journal of Nanoparticle Research. 2005; 7:331–342.
10. Li Q, Mahendra S, Lyon D, Brunet L, Liga M, Li D, Alvarez PJJ. Antimicrobial nanomaterials for water disinfection ans microbial control: Potential applications and implications Water Research. 2008; 42:4591–4602.
11. Kim J, Van der Bruggen B. The use of nanoparticles in polymeric and ceramic membrane structures: Review of manufacturing procedures and performance improvement for water treatment. Environmental Pollution. 2010:1–15.
12. Liu X, Qi S, Li Y, Yang L, Cao B, Tang CY. Synthesis and characterization of novel antibacterial silver nanocomposite nanofiltration and forward osmosis membranes based on layer-by-layer assembly. Water Research. 2013; 47:3081–3092. [PubMed: 23561500]
13. Morones JR, Elechiguerra JL, Camacho A, Holt K, Kouri JB, Tapia Ramirez J, Yacaman MJ. The bactericidal effect of silver nanoparticles. Nanotechnology. 2005; 16:2346–2353. [PubMed: 20818017]
14. Sondi I, Salopek-Sondi B. Silver nanoparticles as antimicrobial agent: a case study on E.coli as a model for Gram-negative bacteria. Journal of Colloid and Interface Science. 2004; 275:177–182. [PubMed: 15158396]
15. Feng QL, Wu J, Chen GQ, Cui FZ, Kim TN, Kim JO. A mechanistic study of the antibacterial effect of silver ions on Escherichia coli and Staphylococcus aureus. J Biomed Mater Res. 2000; 52:662–668. [PubMed: 11033548]
16. Xiu, Zong-ming; Zhang, Qing-bo; Puppala, Hema L.; Colvin, Vicki L.; Alvarez, PJJ. Negligible Particle-Specific Antibacterial Activity of Silver Nanoparticles. Nano Letter. 2012; 12:4271–4275.
17. Zodrow K, Brunet L, Mahendra S, Li D, Zhang A, Li Q, Alvarez PJ. Polysulfone ultrafiltration membranes impregnated with silver nanoparticles show improved biofouling resistance and virus removal. Water Research. 2009; 43:715–723. [PubMed: 19046755]
18. Taurozzi J, Arul H, Bosak VZ, Burban AF, Voice TC, Bruening ML, Tarabara VV. Effect of filler incorporation route on teh properties of polysulfone-silver nanocomposite membranes of different porosities. Journal of Membrane Science. 2008; 325:58–68.
19. Deng Y, Dang G, Zhou H, Rao X, Chen C. Preparation and characterization of polyimide membranes containing Ag nanoparticles in pores distributing on one side. Materials Letters. 2008; 62:1143–1146.
20. Hoek E, Ghosh A, Huang X, Liong M, Zink J. Physical-chemical properties, separtaion performance, and fouling resistance of mixed-matrix ultrafiltration membranes. Desalination. 2011; 283:89–99.
21. Basri H, Ismail AF, Aziz M. Polyethersulfone (PES)–silver composite UF membrane: Effect of silver loading and PVP molecular weight on membrane morphology and antibacterial activity. Desalination. 2011; 273:72–80.
22. Basri H, Ismail AF, Aziz M, Nagai K, Matsuura T, Abdullah MS, Ng BC. Silver-filled polyethersulphone membranes for antibacterial applications - Effect of PVP and TAP addition on silver dispersion. Desalination. 2010; 261:264–271.

23. Chen Y, Zhang Y, Zhang H, Liu J, Song C. Biofouling control of halloysite nanotubes-decorated polyethersulfone ultrafiltration membrane modified with chitosan-silver nanoparticles. Chemical Engineering Journal. 2013; 228:12–20.
24. Sawada I, Fachrul R, Ito T, Ohmukai Y, Maruyama T, Matsuyama H. Development of a hydrophilic polymer membrane containing silver nanoparticles with both organic antifouling and antibacterial properties. Journal of Membrane Science. 2012; 387–388:1–6.
25. Mauter MS, Wang Y, Okemgbo KC, Osuji cO, Giannelis EP, Elimelech M. Antifouling ultrafiltration membranes via Post-Fabrication Grafting of Biocidal nanomaterials. Applied Materials & Interfaces. 2011; 3:2861–2868. [PubMed: 21736330]
26. Liu CX, Zhang DR, He Y, Zhao XS, Bai R. Modification of membrane surface for anti-biofouling performance: Effcet of anti-adhesion and anti-bacteria approches. Journal of Membrane Science. 2010; 346:121–130.
27. Lee SY, Kim H, Patel R, Im S, Kim JB, Min BR. Silver nanoparticles immobilized on thin film composite polyamide membrane: characterization, nanofiltration, antifouling properties. Polymer Advanced Technology. 2007; 18:562–568.
28. Zhu X, Tang L, Wee K-H, Zhao Y-H, Bai R. Immobilization of silver in polypropylene membrane for anti-biofouling performance. Biofouling: The Journal of Bioadhesion and Biofilm Research. 2011; 27:773–786.
29. Schmittgens R, Wolf M, Schultheiss E. A versatile system for large area coating of nanocomposite thin film. Plasma Process. Polym. 2009; 6:S912–S916.
30. Wolf M, Schmittgens R, Nocke A, Hecker D, Liepelt M, Schultheiss E. Plasma deposition of condutive polymer composites for strain sensor applications. Procedia Chemestry. 2009; 1:879–882.
31. Shadpour H, Musyimi H, Chen J, Soper S. Physiochemical properties of various polymer substrates and their effects on microchip electrophoresis performance. J. Chromatogr. A. 2006; 1111:238–251. [PubMed: 16569584]
32. Zhou J, Li W, Gu J-S, Yu H-Y. Surface modification of polypropylene membrane to improve antifouling characteristics in a submerged membrane-bioreactor: Ar plasma treatment. Membrane Water Treatment. 2010; 1:83–92.
33. Hongquan J, Manolache S, Wong ACL, Denes FS. Plasma-Enhanced Deposition of Silver Nanoparticles onto Polymer and Metal Surfaces for the Generation of Antimicrobial Characteristics. Journal of Applied Polymer Science. 2004; 93:1411–1422.
34. Joyce J, Giudice MD, Weaver JH. Quantitative analysis of synchrotron radiation photoemission core level data. Journal of Electron Spectroscopy and Related Phenomena. 1989; 49:31–45.
35. Beamson, G.; Briggs, D. High Resolution XPS of Organic Polymers. London: Wiley; 1992.
36. Moulder, J.; Strickle, W.; Sobol, P.; Bomben, K. Handbook of X-ray Photoelectron Spectroscopy. Minnesota: Perkin-Elmer Corporation; 1992.
37. Choi O, Hu Z. Size dependent and reactive oxygen species related nanosilver toxicity to nitrifying bacteria. Environmental Science and Technology. 2008; 42:4583–4588. [PubMed: 18605590]
38. Pradeep T, Anshup. Noble metal nanoparticles for water purification: A critical review. Thin solid film. 2009; 517:6441–6478.
39. Lopez-Perez P, Marques A, Silva Rd, Pashkuleva I, Reis R. Effect of chitosan membrane surface modification via plasma induced polymerization on the adhesion of osteoblast-like cells. J. Mater Chem. 2007; 17:4064–4071.
40. Saxena N, Prabhavathy C, De S, DasGupta S. Flux enhancement by argon–oxygen plasma treatment of polyethersulfone membranes. Separation and Purification Technology. 2009; 70:160–165.
41. Gröning P, Collaud-Coen M, Kütttel OM, Schlapbach L. Influence of gas pressure on the plasma reaction on polyethersulphone. Applied surface science. 1996; 103:79–89.
42. Hopkins J, Badyal JPS. Plasma modification of Polyethersulfone. Macromolecules. 1994; 27:5498–5503.
43. WHO. Background document for development of WHO Guidelines for Drinking-water Quality. Geneva: World Health Organization; 2004. Silver in drinking water.

44. Ochoa NA, Masuelli M, Marchese J. Effect of hydrophilicity on fouling of an emulsified oil wastewater with PVDF/PMMA membranes. Journal of Membrane Science. 2003; 226:203–211.

45. Tarabara, VV. Multifunctional nanomaterial-enabled membranes for water treatment. William Andrew Inc.; 2009.

46. Vrouwenvelder JS, Manolarakis SA, Hoekd JPvd, Paassen JAMv, Meer WGJvd, Agtmaal JMCv, Prummel HDM, Kruithof JC, Loosdrecht MCMv. Quantitative biofouling diagnosis in full scale nanofiltration and reverse osmosis installations. Water Research. 2008; 42:4856–4868. [PubMed: 18929382]

Highlights

- Modified UF membranes were obtained using a unique plasma reactor.
- Bactericidal membranes were obtained by GFS deposition of silver nanoparticles.
- PECVD deposition of a thin layer of PMMA enhanced the fixation of silver nanoparticles.
- Anti-adhesion and bactericidal assays were tested successfully in modified membranes.
- Treated membranes revealed effective resistance to biofouling during water disinfection by UF.

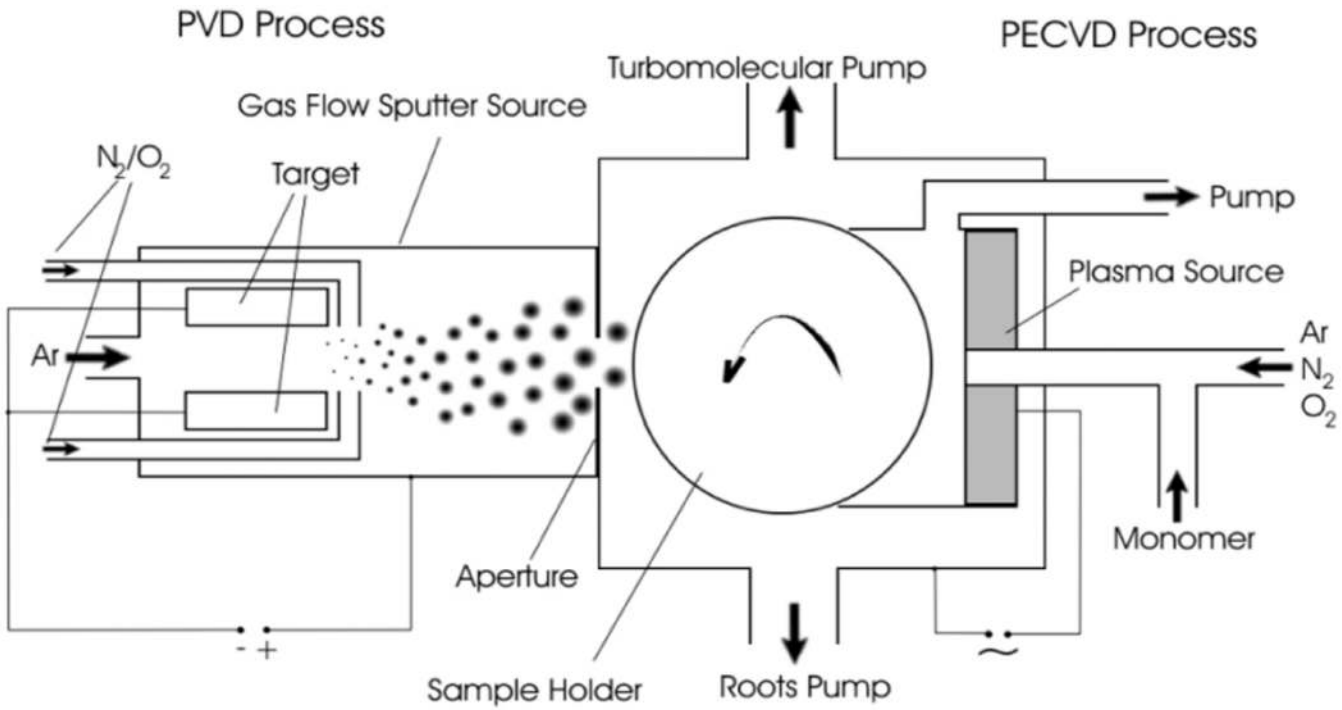

Figure 1.

Schematic of nanocomposite deposition system consisting of a GPC unit for nanoparticle fabrication (left unit), a PECVD source for the matrix material deposition (right unit), and a rotating sample holder to transport the sample between the two sources [30].

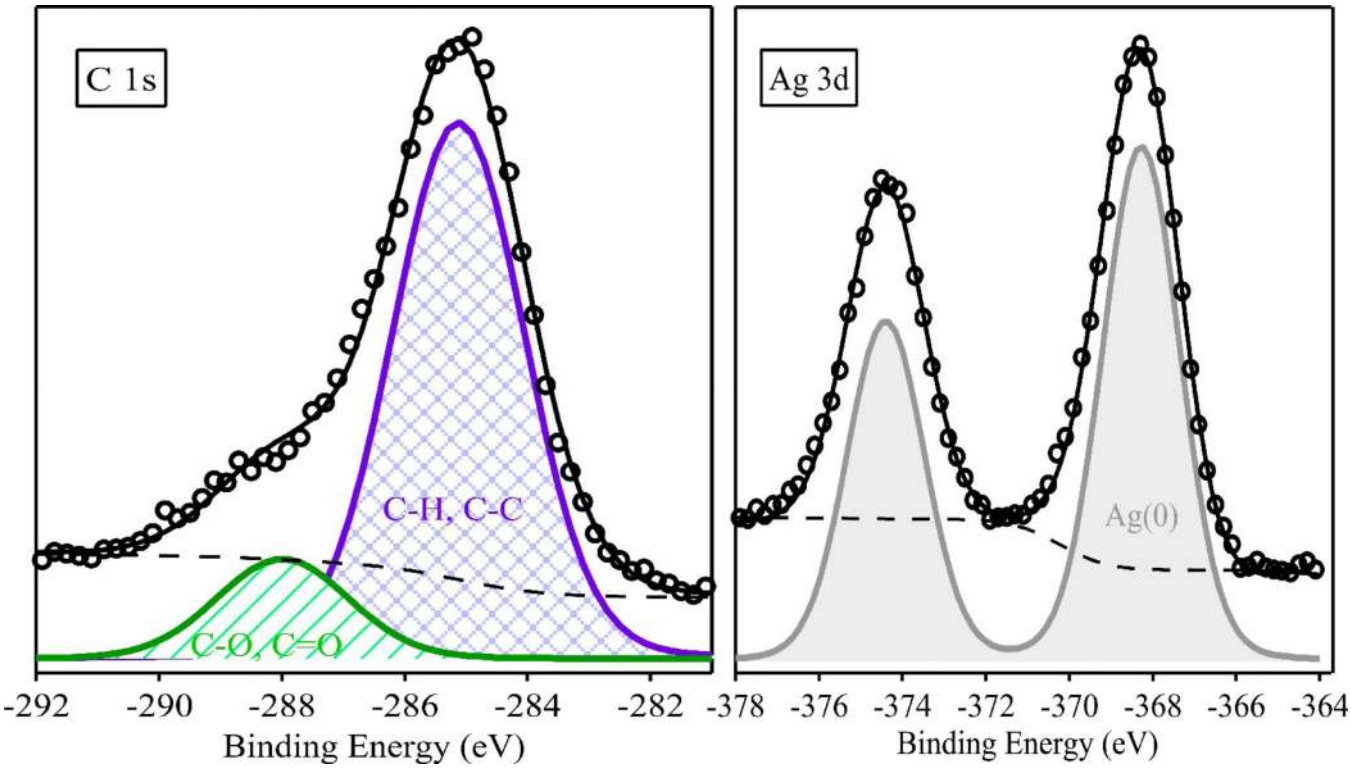

Figure 2.

XPS peaks of C 1s and Ag 3d corresponding to the sample M4. Symbols are used for experimental data, plain line for fitting, and dashed line for Shirley-type background. Shaded areas represent subtracted photoemission peaks.

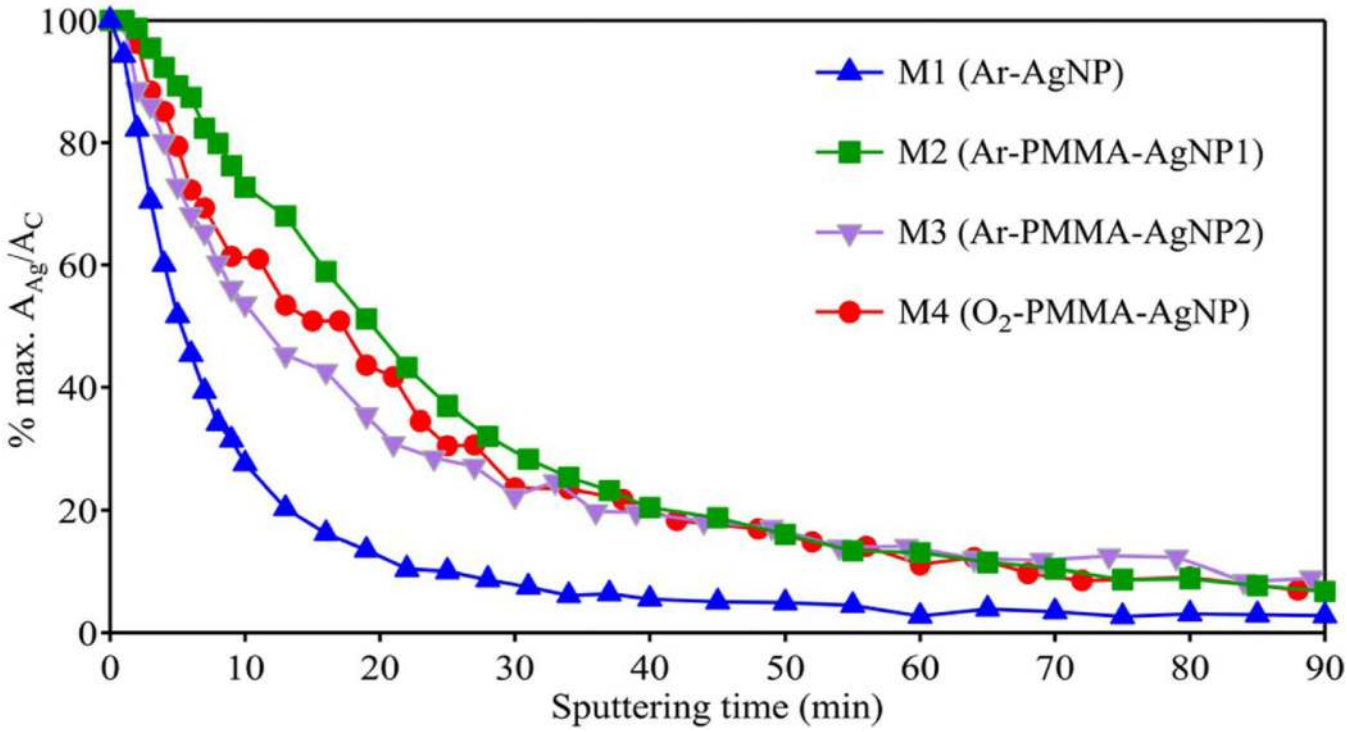

Figure 3.

Depth profile composition analysis of non-washed samples (M1–M4). Ag 3d to C 1s area ratios (A_{Ag}/A_C) are normalized to the maximum Ag value.

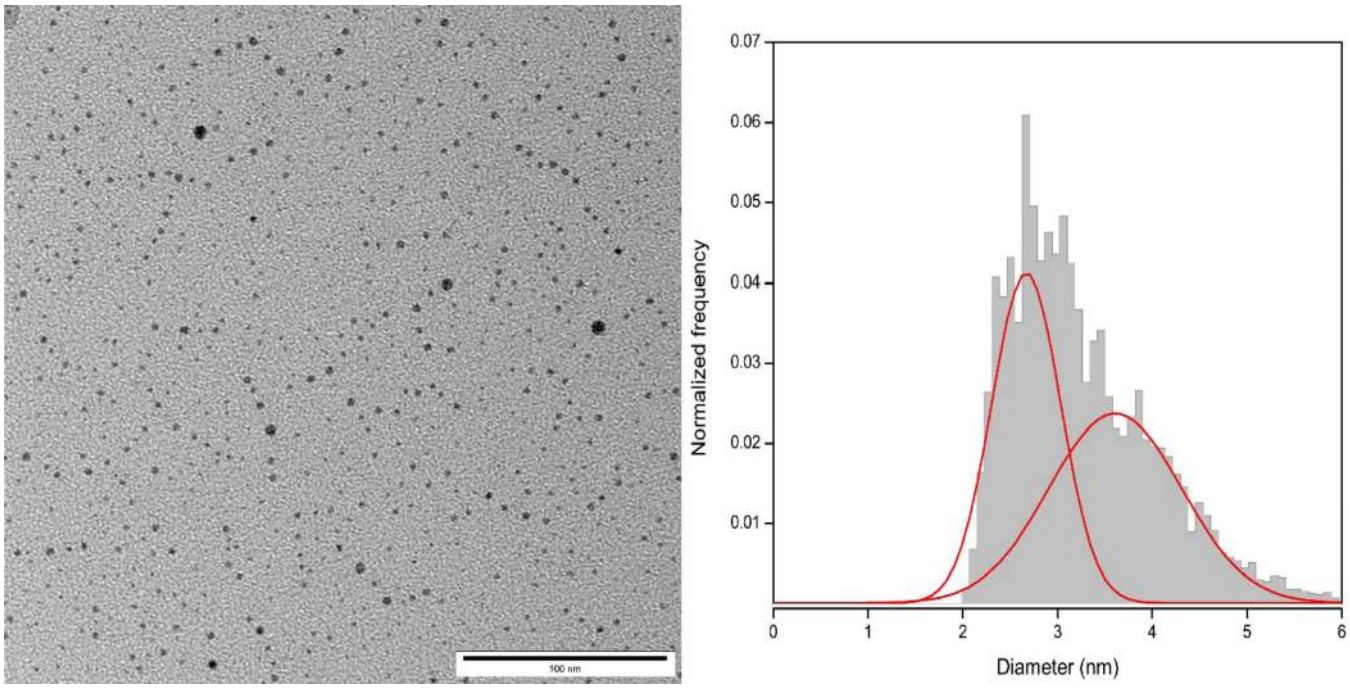

Figure 4.

TEM micrograph of silver nanoparticles deposited onto a silicon wafer under the same conditions used for the modified membranes used in this work. The histogram shows the nanoparticle size distribution fitted by two Gaussian curves.

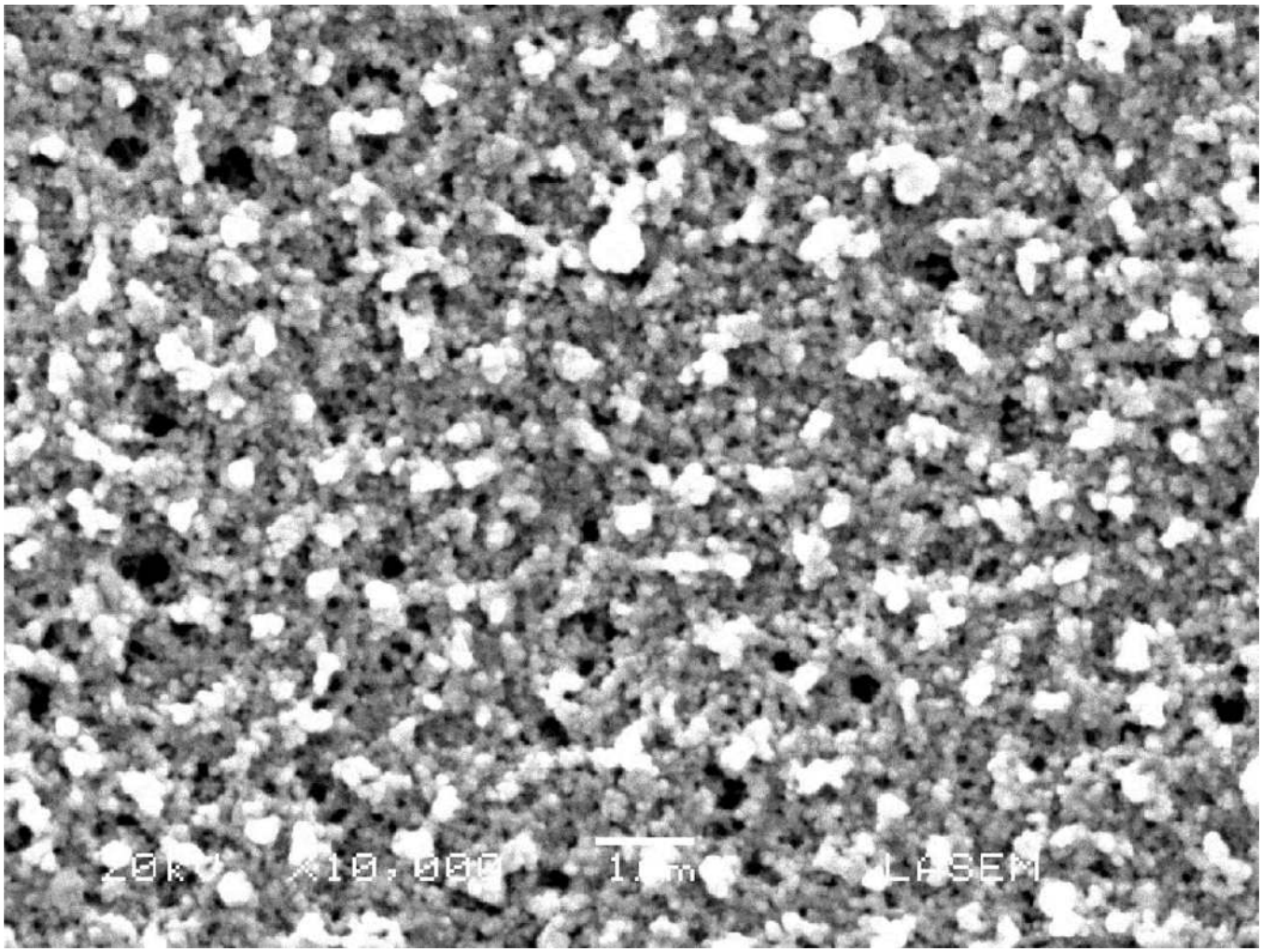

Figure 5.

SEM image of membrane treated with Ar/O_2 plasma (2 min of exposition) and SNP deposition (20 s of exposition) without PMMA. The permeability of this membrane was 742.0 $l.m^{-2}\cdot h^{-1}.bar^{-1}$, almost three times higher than the virgin membrane. Rejection capacity was lost in this membrane due to its high permeability and several and large pores that were observed by SEM; thus, it was not subjected to bactericidal analysis.

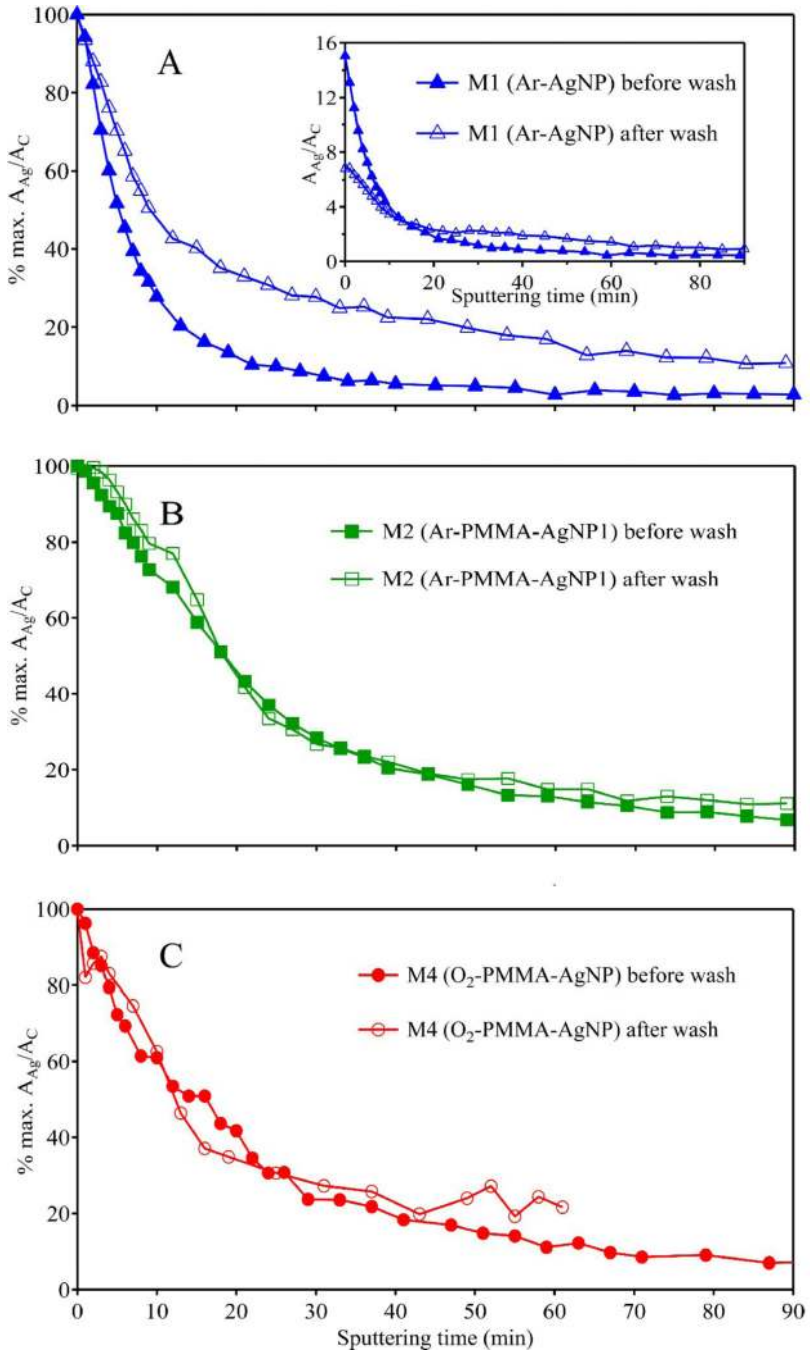

Figure 6.

Depth profile analysis of the normalized (to the maximum Ag value on the surface) Ag 3d to C1s ratios (A_{Ag}/A_C) for: M1 (A), M2 (B) and M4 (C). The inset in the top panel (A) shows the Ag to C ratio in absolute values for washed (open symbols) and non-washed (full symbols) sample.

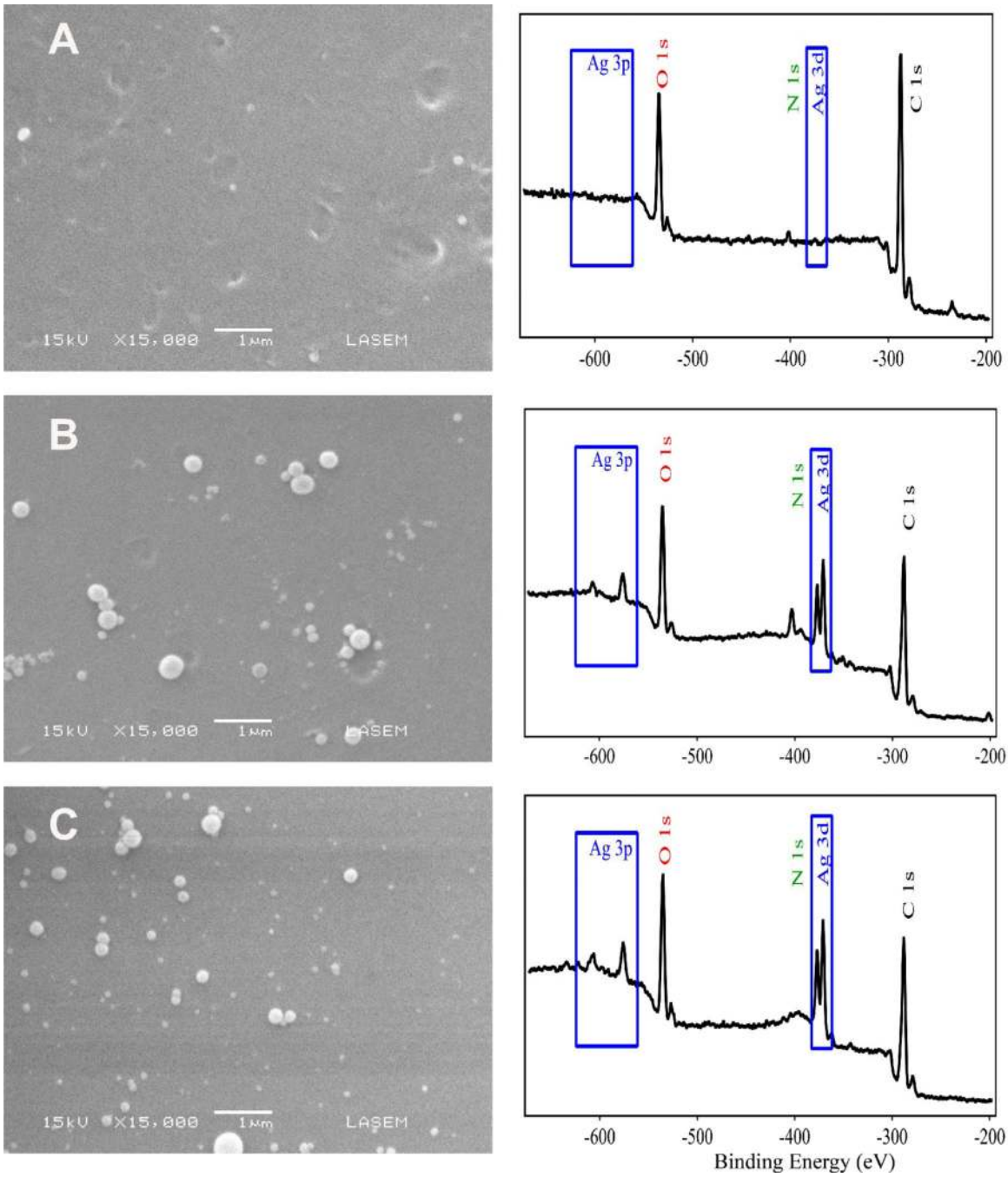

Figure 7.

SEM images (15,000×) (left side) and XPS spectra (right side) of the samples from top to bottom A: Virgin membrane without treatment (PES), B: M3 (Ar-PMMA-SNP), and C: M4 (Ar/O_2-PMMA-SNP).

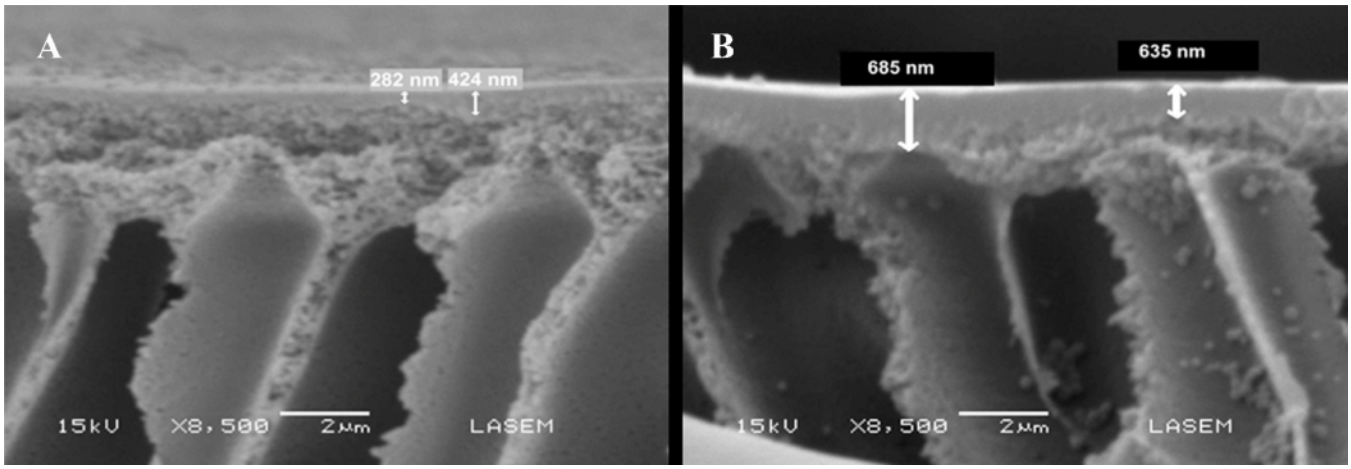

Figure 8.

SEM micrographs of M3 (A) and M4 (B) membrane cross-sections. Figure shows fingerlike pore morphology and the PMMA layer thickness.

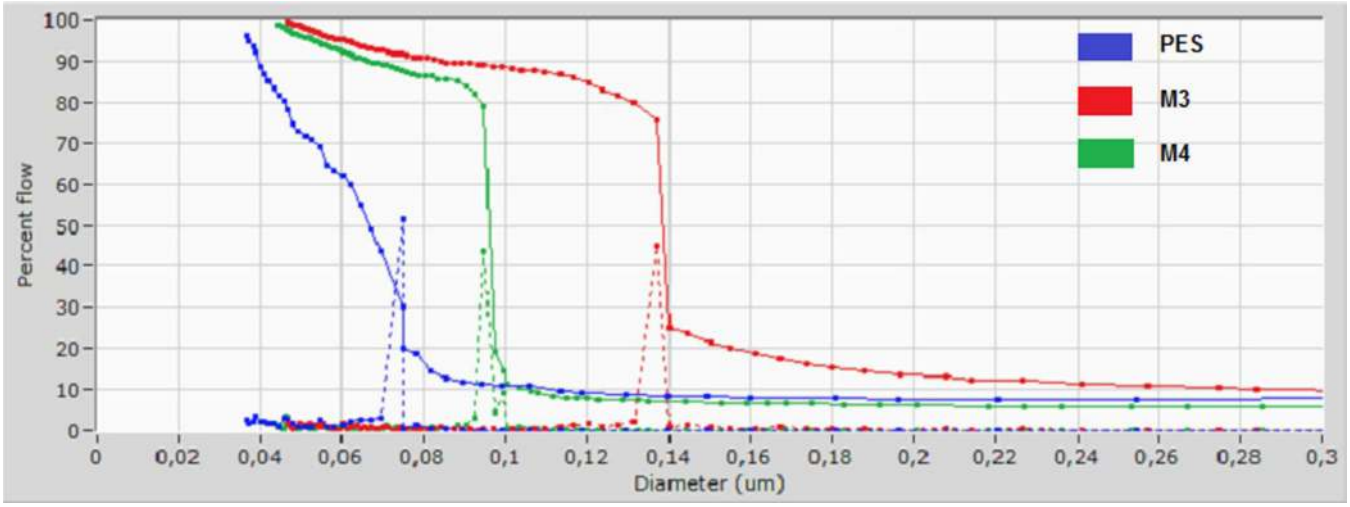

Figure 9.

Pore size distribution of PES (untreated), M3 and M4 membranes obtained by bubble point method with a Porolux™ 1000 (POROMETER nv). The graph is represented in terms of gas flow and cumulative flow (%) versus pore size diameter.

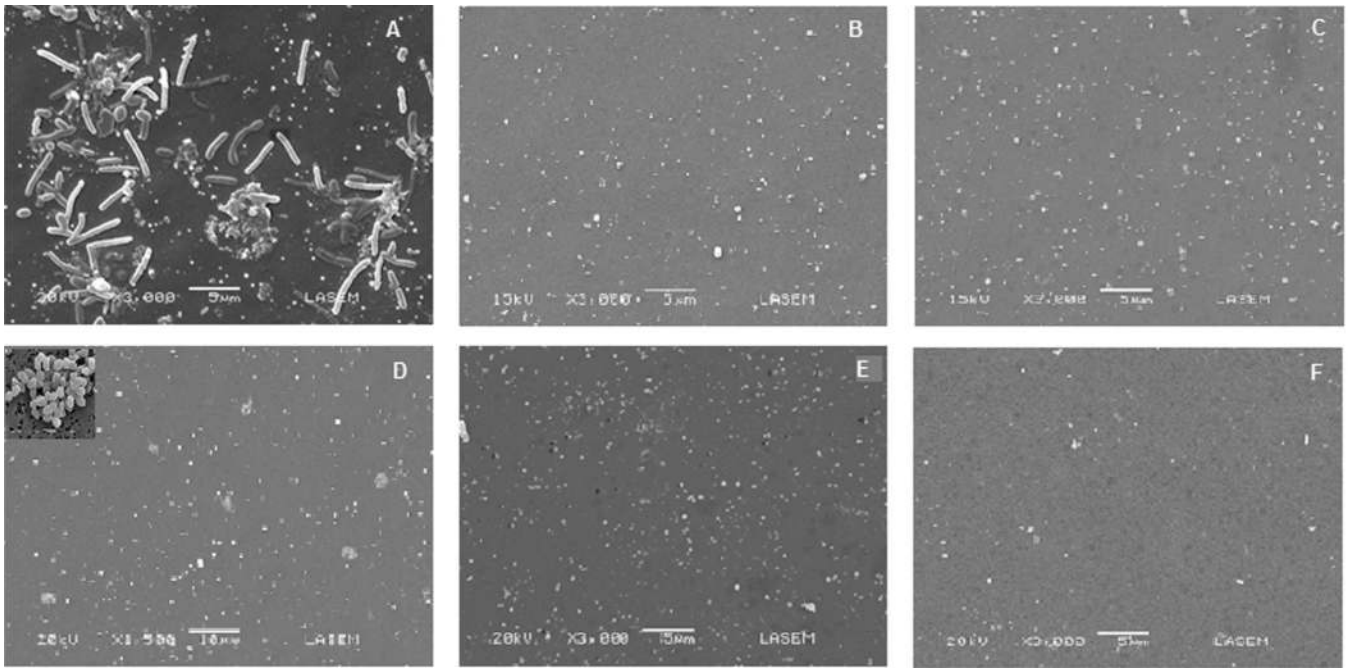

Figure 10.

SEM images for adhesion tests. From *Salmonella* Typhimurium suspension, A: virgin membrane B: M3 and C: M4. From *Enterococcus faecalis* suspension, D: virgin, E: M3 and F: M4 membranes.

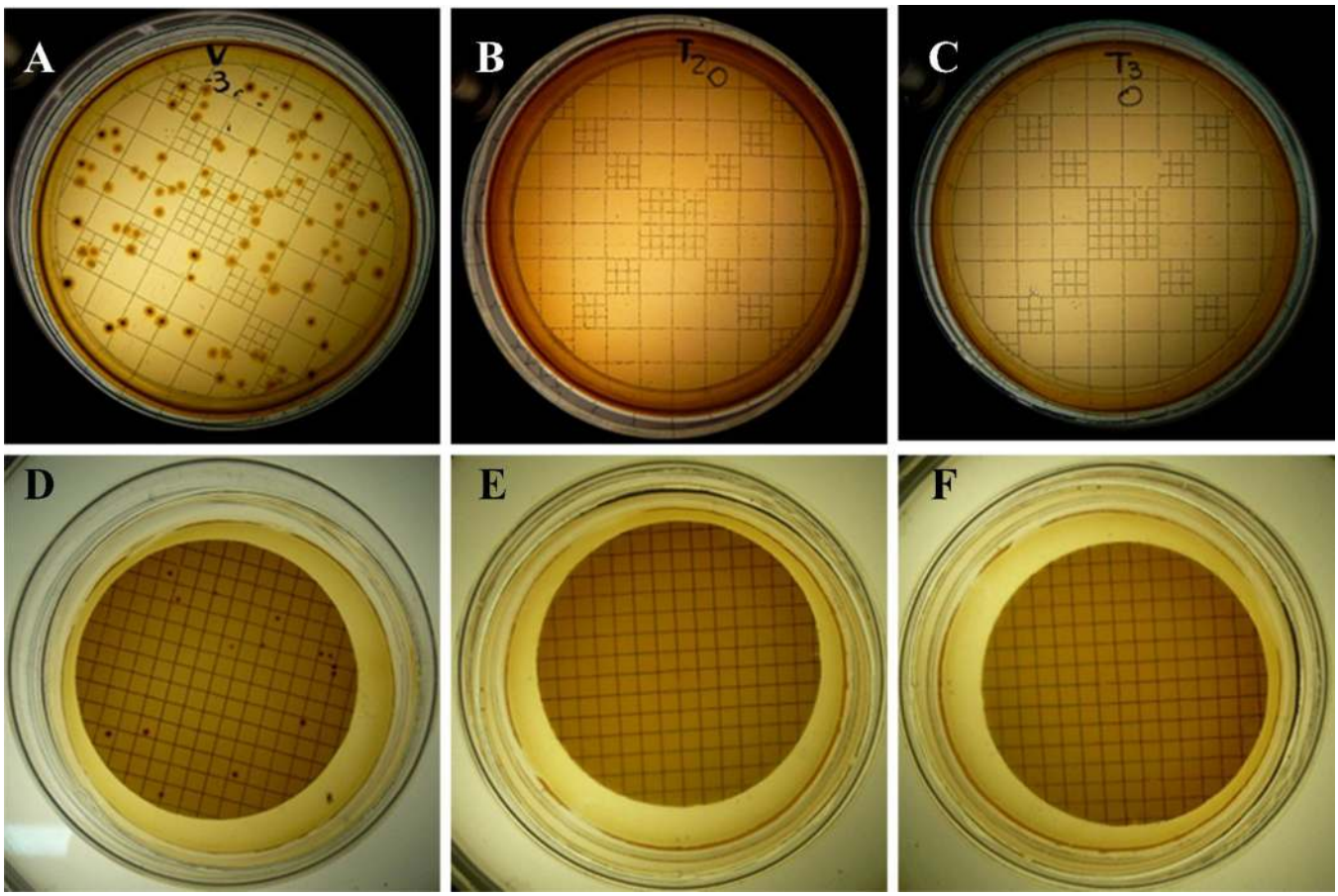

Figure 11.

Viable *S.* Typhimurium grown on SS agar plate from suspension in contact with A: untreated (dilution 10^{-3}), B: M3 and C: M4 membranes, undiluted. Viable *E. faecalis* bacteria grown on mE agar from suspensions in contact with D: untreated (dilution 10^{-2}), E: M3 and F: M4 membranes, undiluted.

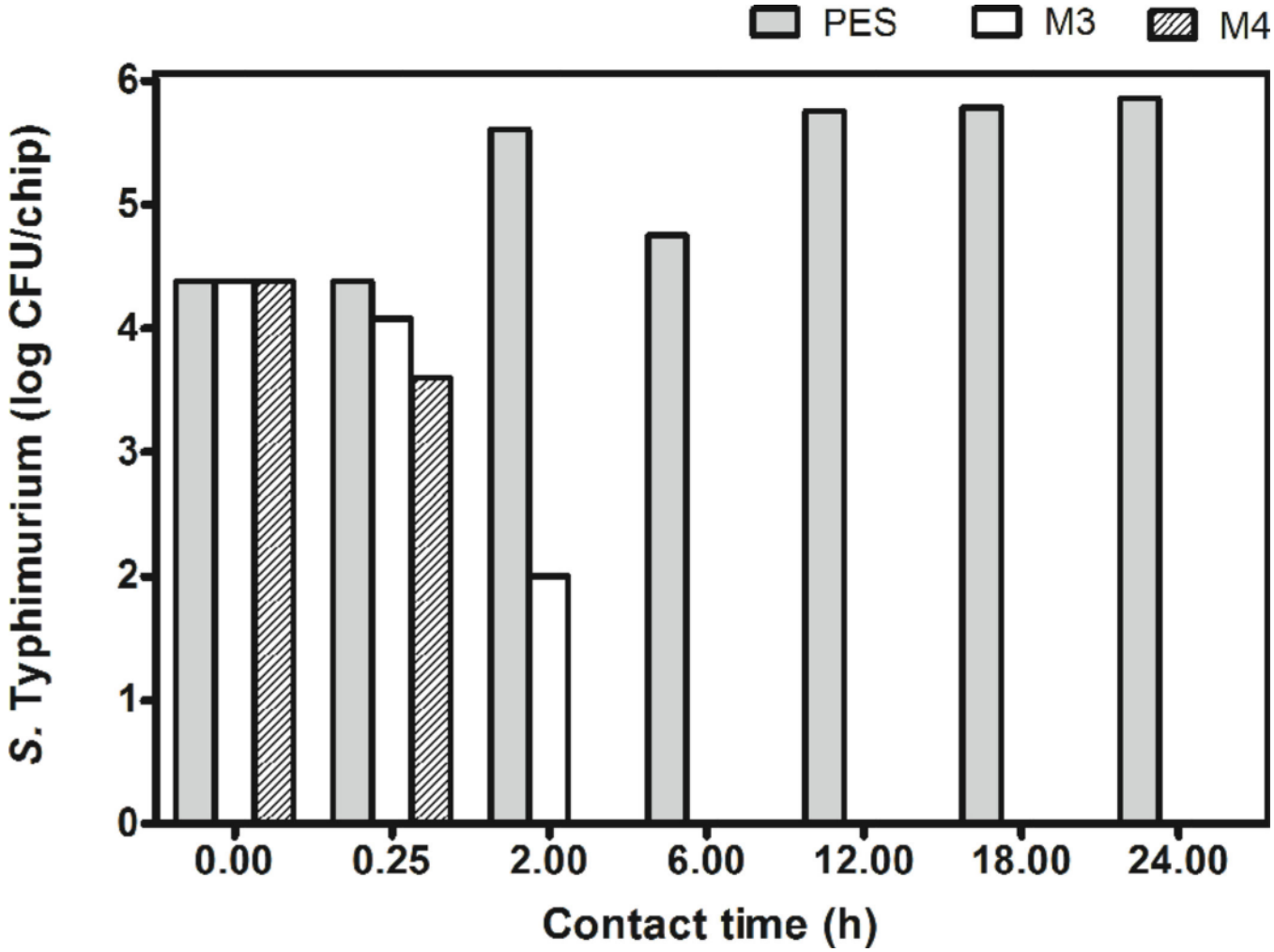

Figure 12.
Bactericidal effect of SNP on *Salmonella* Typhimurium

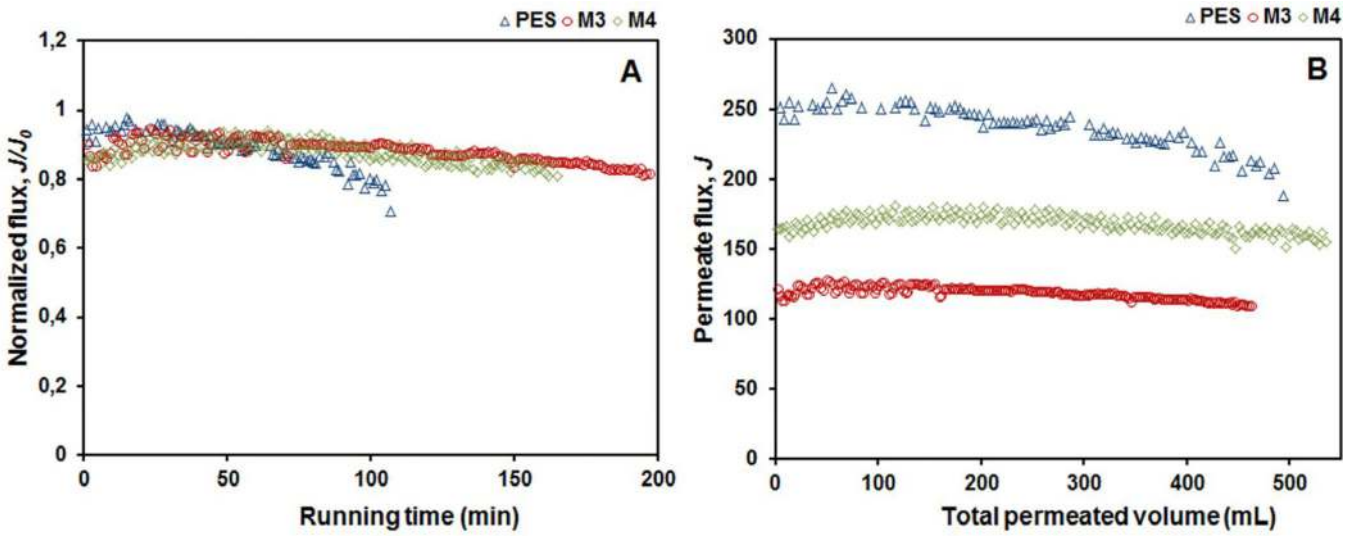

Figure 13.

Ultrafiltration of 1 l of *Salmonella* Typhimurium (1×10^6 CFU/ml) and *Enterococcus faecalis* (1×10^5 CFU/ml) suspensions for treated (M3 and M4) and untreated (PES) membranes. A. Normalized flux with time. B. Variation of permeate flux ($l.m^{-2}\ h^{-1}$) with accumulated volume.

Table 1

Experimental conditions for plasma activation with Argon (Ar) on M1, M2, and M3 and with Argon and Oxygen mix (Ar/O_2) on M4

Gas	Ar	Ar/O_2
Pressure [Pa]	10	10
Flow [sccm]	50	20/30
Power [Watts]	100	50
Time [min]	2	1

Table 2

Morphological and transport properties of modified (M3 and M4) and non-modified (PES) membranes.

Property	PES	M3	M4
Compaction factor	2.65	1.98	6.09
Permeability [$l.m^{-2}.h^{-1}.bar^{-1}$]	255.0 ± 17.0	132.0 ± 1.6	157.0 ± 3.3
Contact angle [°]	68.90 ± 0.10	37.10 ± 0.17	62.40 ± 0.60
Work of adhesion [$mJ.m^{-2}$]	99.01 ± 0.12	130.90 ± 0.13	106.60 ± 0.68
Surface energy [$mJ.m^{-2}$]	42.390 ± 0.006	60.90 ± 0.09	46.40 ± 0.37
Pore size [μm]	0.0668	0.1387	0.0960
Pore structure factor [m^{-1}]	5079.66	609.91	1700.16